Electronic Supplementary Material (ESI) for Nanoscale.
This journal is © The Royal Society of Chemistry 2019

Supplementary Material

Out-of-plane ion transport makes nitrogenated holey graphite a promising high-rate anode for both Li and Na ion batteries

He Huang,[b] Hong-Hui Wu,[c] Cheng Chi,[b] Jiaming Zhu,[d] Baoling Huang,[b*] Tong-Yi Zhang[a*]

[a] Materials Genome Institute, Shanghai University, 333 Nanchen Road, Shanghai 200444, China.

[b] Department of Mechanical and Aerospace Engineering, Hong Kong University of Science and Technology, Clear Water Bay, Kowloon, Hong Kong, China.

[c] Beijing advanced innovation center for materials genome engineering, State Key Laboratory for Advanced Metals and Materials, University of Science and Technology Beijing, Beijing 100083, China.

[d] Department of Mechanical Engineering, Hong Kong Polytechnic University, Hong Kong, China.

Note 1: Structural and electronic properties of C_2N-NHG monolayer

The optimized structure of the NHG monolayer is shown in Figure S1. Similar to C_3N monolayer,[1] C_2N-NHG monolayer is a two-dimensional crystal consisting of carbon and nitrogen atoms, an extension of nitrogenated holey graphene. It shows a planar network structure that possesses evenly distributed carbon holes of a diameter of 5.51 Å, of which the edge is decorated by nitrogen atoms. The first principles calculation predicts the C_2N-NHG monolayer with a lattice constant of 8.33 Å, in good agreement with reported results in previous literatures.[2-4] Shown in the inset of Figure S1, each hexagonal primitive unit cell of NHG includes 6 nitrogen and 12 carbon atoms and therefore it has the stoichiometry of C_2N. In the 2D structure, the C-N bond length is 1.34 Å, while the C-C bonds have two different values: the bond at the border of the hole is 1.47 Å (C-C(1)) and the shared bond between pyrazine and benzene rings is 1.43 Å (C-C(2)). Here short C-C and C-N bond lengths show that the C_2N-NHG monolayer structure is formed through strong carbon-nitrogen hybridization and the benzene rings still have graphitic character, which is revealed in the shared electron accumulation between the C and N atoms (see Figure S2(a)). The bader charge analysis shows the 0.54 electron loss of C atom and 1.08 electron gain of N atom, respectively. Therefore, the electron accumulation right in the center of C-C bonds and shared electron density partially to N atoms of C-N bonds form the *sp*2 hybridization of the C_2N-NHG monolayer.

The phonon dispersion and AIMD simulation are conducted to certify the structural and thermodynamic properties of the C_2N-NHG monolayer at 0 K and elevated temperatures. Determination of the phonon properties of a given material not only allows us to examine its dynamical stability but also to find out the characteristic fingerprints of the structure. Shown in Figure S2(b), all positive phonon dispersions demonstrate the structural stability of C_2N-NHG monolayer at 0 K. Meanwhile, depicted in Figures S3 and S4, the steady constant total energy and very small values of mean square displacements of C atoms and N atoms at room and high temperatures demonstrate the thermodynamic stability of the C_2N-NHG monolayer over a wide temperature range.

The electronic structure calculation shown in Figure S2(c) indicates that the C_2N-NHG monolayer is a semiconductor with a direct band gap of 1.66 eV. Our result is consistent with earlier theoretical studies[3-5] but exhibits a smaller electronic band gap than the experimentally measured value of 1.96 eV.[4] The underestimation of band gap by DFT is normal due to its ground state nature. The partial density of states (PDOS) indicate the *p*-orbitals of both C and N atoms contribute to the total DOS of C2N-NHG monolayer.

Note 2: Li/Na adsorption and diffusion on C_2N-NHG monolayer

We first studied the adsorption performance of Li and Na atoms on C_2N-NHG monolayer. For the C_2N-NHG 2×2×1 supercell monolayer, for both Li and Na atoms there are three stable adsorption sites: the hollow site above the center of the inter-hole (Site 1), the hollow site above the center of benzene ring (Site 2), and the hollow site above the center of pyrazine ring (Site 3), and for Li atoms only there is another stable site: the hollow site 0.77 Å deviating from the center of the hole (Site 4, see Figures S1 and S4). The other six possible adsorption sites mentioned in Wu et al.'s paper[6] are found unstable and atoms at those sites would automatically move to the above four sites. In particular, Na atom on Site 4 is found unstable and prefers to move to the Site 1 of the C_2N-NHG monolayer. The corresponding adsorption energies and adsorption distances on the C_2N-NHG monolayer at different adsorption sites are obtained from the first-principles optimization and are summarized in Table 1. With similar adsorption energies, the most stable site for Li atom adsorption is Site 4, 0.77 Å deviated from the center of inner-hole. However, the adsorption site in the center of the inter-hole is the most stable one for Na atom. In both cases, the optimal adsorption distances are zero from the C_2N-NHG monolayer. The large adsorption energy indicates the C_2N-NHG monolayer has great adsorption ability of Li/Na atoms, meanwhile it implies it is difficult for Li or Na atoms to diffuse away from the inter-holes due to the deep potential well. For both Site 2 and Site 3, the adsorption energies are quite small and even positive, indicating these two transitional sites are intrinsically not stable. The adsorption distance to C_2N-NHG monolayer at Site 2 and Site 3 are similar, with the values of about 1.7 Å for Li atom and 2.2 Å for Na atom. The adsorption ability for Li/Na atom on C_2N-NHG monolayer is found much stronger than that on C_3N monolayer,[7] which may be ascribed to the electron accumulation of the inter-holes in C_2N-NHG monolayer. It is found that large charge transfer occurs between Li/Na atom and C_2N-NHG monolayer at Site 1(see Figure S6). The bader charge analysis indicates Li atom and Na atom lose 0.931 and 0.932 electrons to the C_2N-NHG monolayer, respectively. The electron density of states before and after the adsorption of Li and Na atom on C_2N-NHG monolayer are shown in Figure S7. The significant charge transfer from Li/Na atom to C_2N-NHG monolayer effectively shifts the fermi energy level into the conduction band, resulting in enhanced electrical conductivity of the C_2N-NHG monolayer after Li or Na adsorption.

A facile diffusion of Li/Na atom on the C_2N-NHG monolayer will give a rapid charge-discharge rate for an anode material. From the adsorption energy in Table S1, we find that both Li and Na atoms diffuse on the C_2N-NHG monolayer via the distinct pathway: from the center of inter-hole to the next center of inter-hole, by pathing through the hollow site above the center of benzene ring (Site 1→Site 2→Site 1) with the energy barriers of 2.72 eV and 3.06 eV, respectively. Meanwhile, the diffusion pathway for Li atom along the Site 4 to Site 2 is also investigated with the energy barrier of 2.85 eV. The energy landscapes for Li and Na atom diffusions on C_2N-NHG monolayer are plotted in Figure S8. The calculated energy barriers for single Li and Na diffusions are consistent with the results reported by Wu et al.[6] and Zhang et al.[8] These huge energy barrier values are found too high to overcome during the lithiation and sodiation process, which will severely restrict the charge-discharge rate for an anode material. Compared with other promising 2D anode material, such as Mn_2C (0.27 eV for Li),[9] and MoS_2(0.28 eV for Na),[10] the huge energy barriers caused by the inter-holes of C_2N-NHG monolayer make it difficult to achieve fast in-plane diffusion in the monolayer configuration.

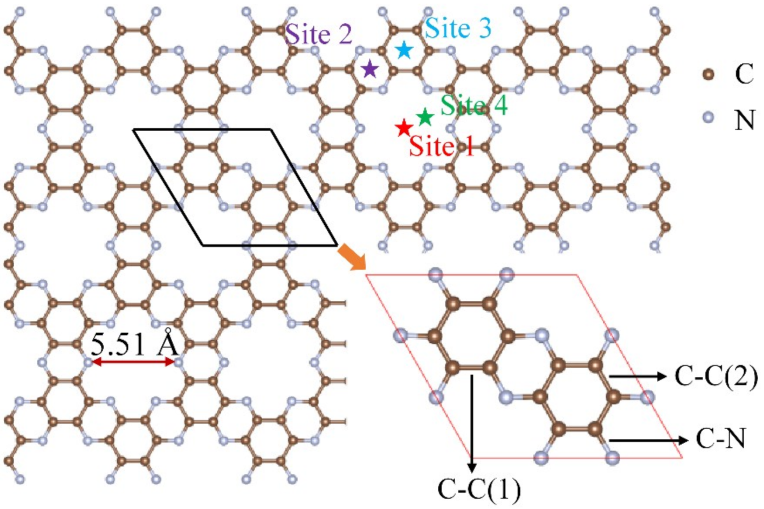

Figure S1. Crystal structure of optimized C_2N-NHG monolayer. Nitrogen and carbon atoms are shown by silver and brown balls, respectively. The inset shows an enlarger hexagonal primitive unit cell of the C_2N-NHG monolayer. The adsorbed sites are labelled as Site 1, Site 2, Site 3 and Site 4.

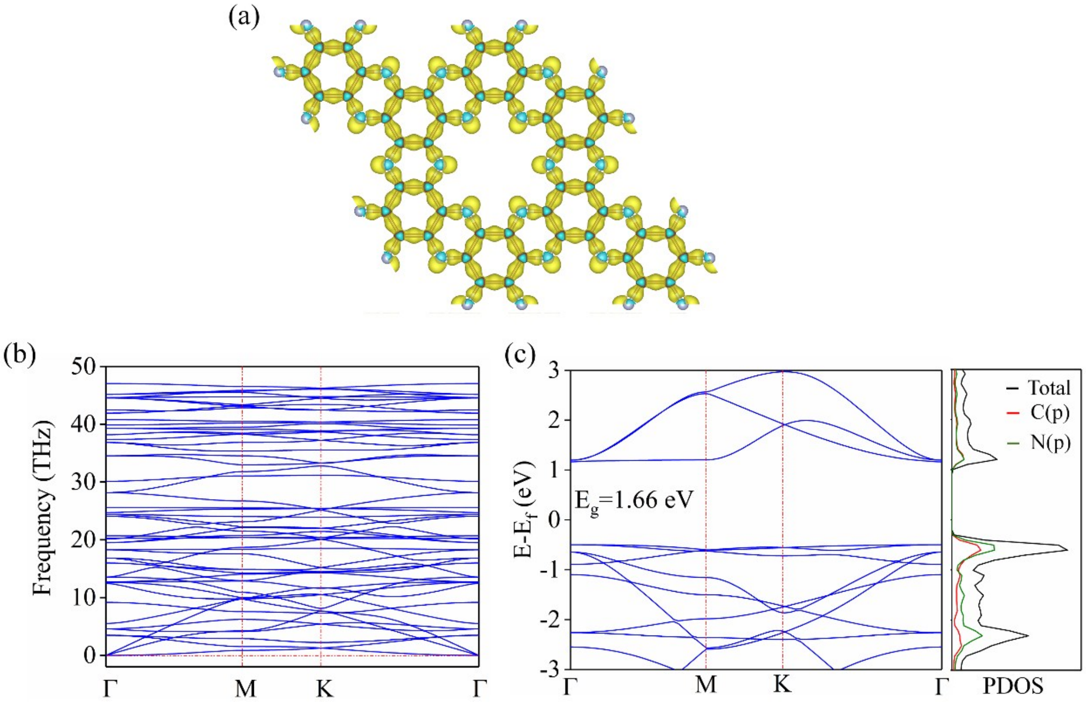

Figure S2. (a) Electron density difference of the C_2N-NHG monolayer. The silver balls represent N atoms and the brown ones represent C atoms. The yellow region indicates electron accumulation and the cyan region indicates electron deficiency. The isosurface value is set to 0.01 e/Bohr3. (b) Phonon dispersion of the C_2N-NHG monolayer. All phonon frequencies are positive values, demonstrating the dynamic stability of NHG monolayer at 0 K. (c) The PBE approached electronic band structure and partial density of states (PDOS) of C_2N-NHG monolayer shows a direct band gap of 1.66 eV. The fermi energy level is set to be 0.

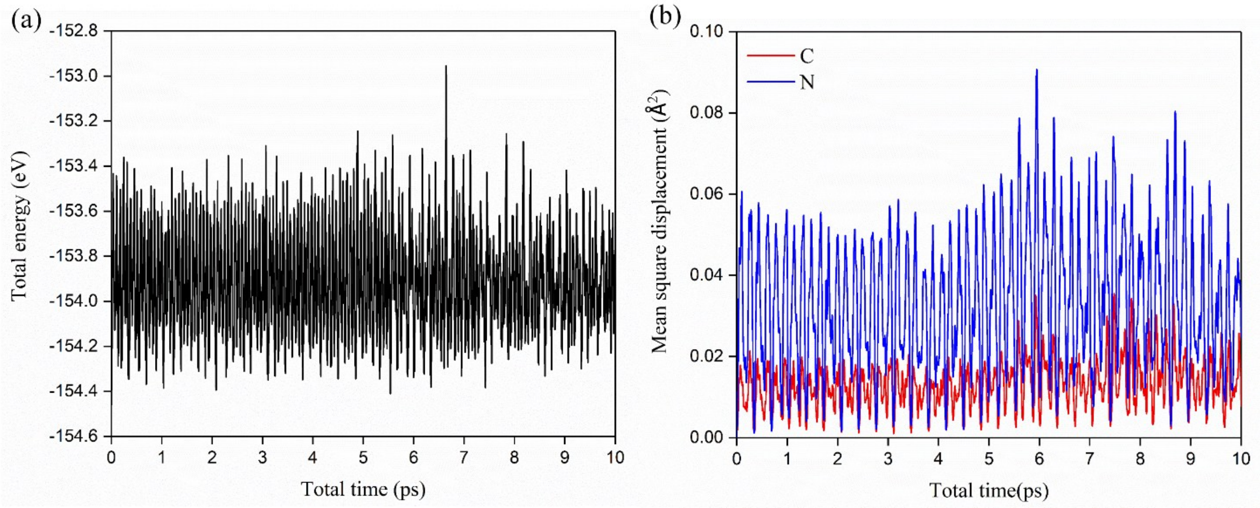

Figure S3. (a) The total energy of the C2N-NHG monolayer vs. total simulation time. (b) The mean square displacements of C atoms and N atoms. The total simulation time is 10 ps and the temperature is set to 300 K.

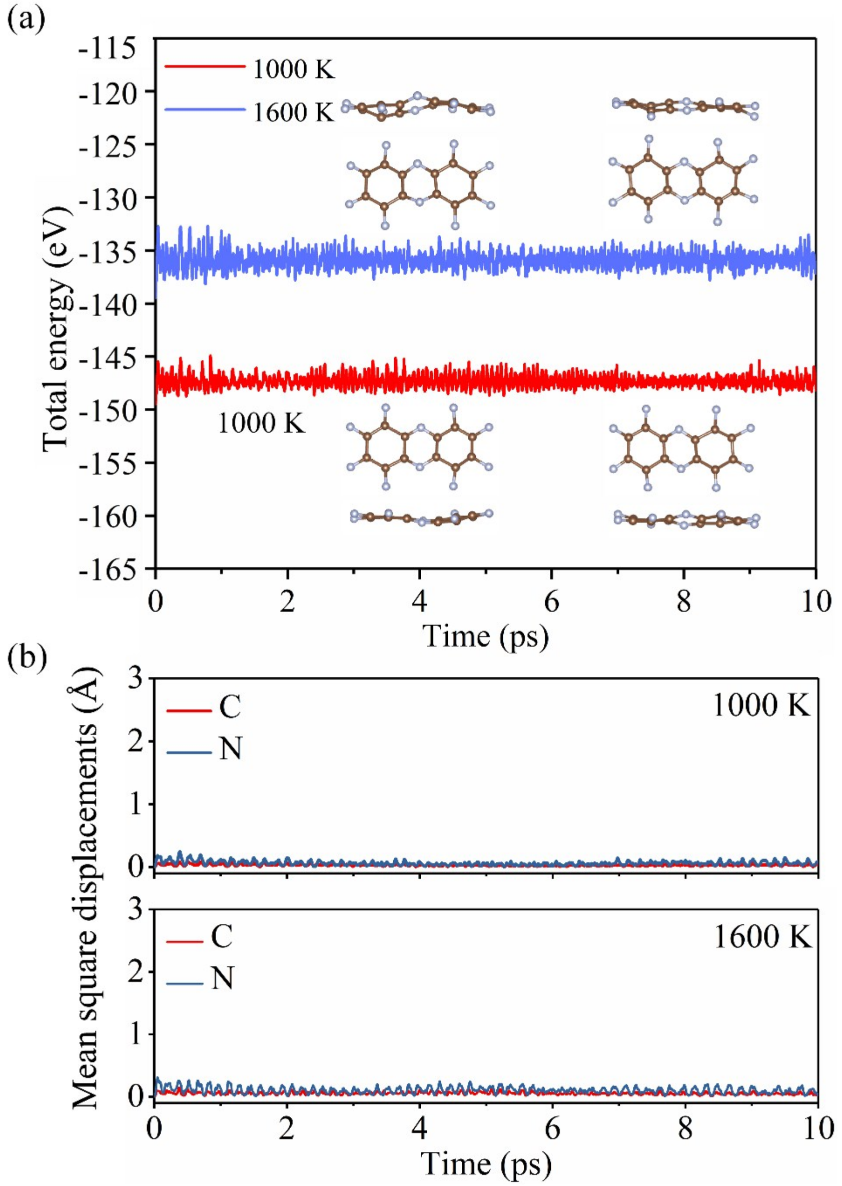

Figure S4. (a) The total energies of the C_2N-NHG monolayer vs. total simulation time at 1000 K and 1600 K. The inset shows the transitional structures of C_2N-NHG monolayer at 4 ps and 8 ps. (b) The mean square displacements of C atoms and N atoms at 1000 K and 1600 K.

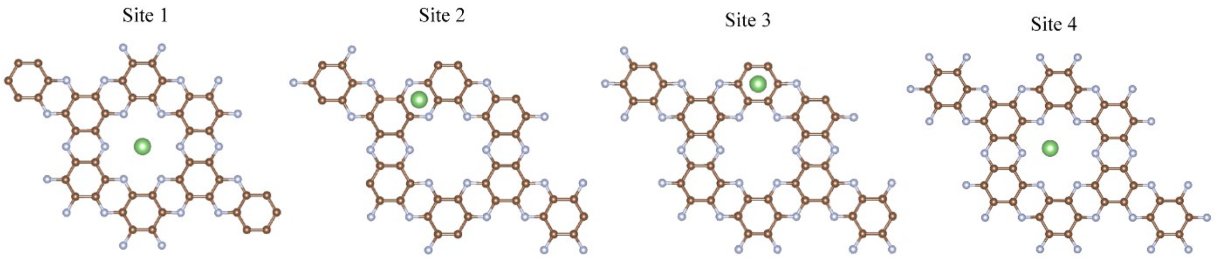

Figure S5. Four kinds of adsorption sites of Li/Na atom on C_2N-NHG monolayer unit cell: the hollow site above the center of the inter-hole (Site 1), the hollow site above the center of benzene ring (Site 2), the hollow site above the center of pyrazine ring (Site 3) for Li/Na, and the hollow site deviating 0.77 Å from the center of the inter-hole (Site 4) for Li only. The green ball represents Li or Na atom, and the silver and brown balls represent nitrogen and carbon atoms, respectively.

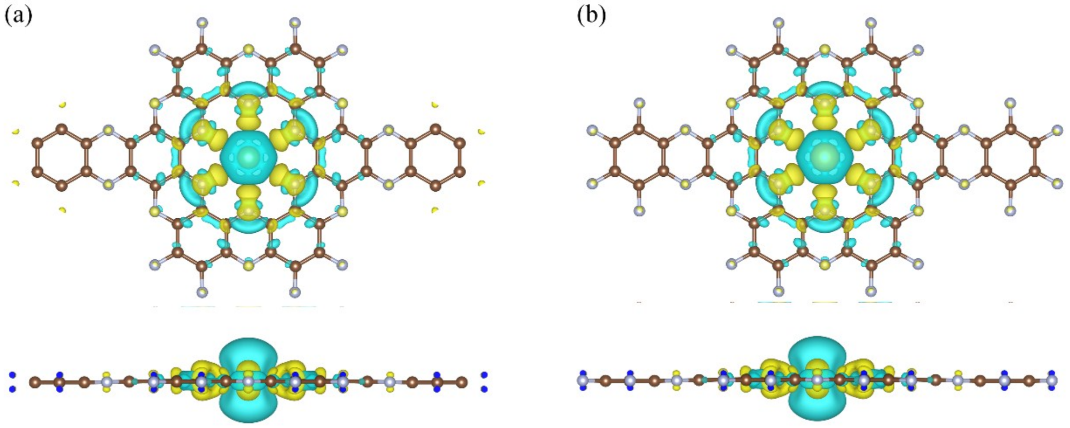

Figure S6. Electron density difference plot of (a) Li atom and (b) Na atom adsorption in the center of C_2N-NHG monolayer inter-hole (Site 1) from top and side views. The yellow regions represent electron gain and the cyan regions represent electron loss. The isosurface value is set to 0.001 e/Bohr^3.

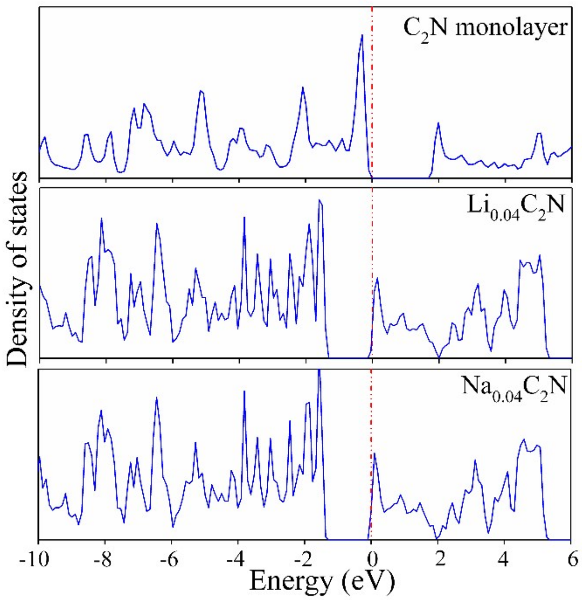

Figure S7. Electron density of states before and after Li/Na single atom adsorption on 2×2×1 C$_2$N-NHG monolayer. The red dot line means Fermi energy level, which is set to 0.

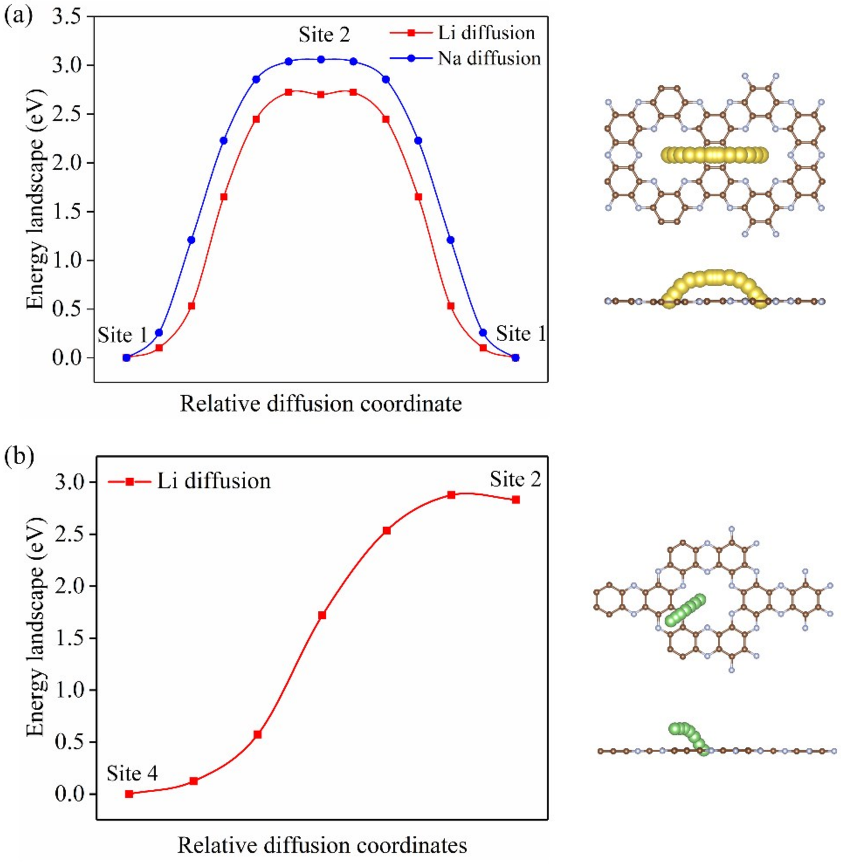

Figure S8. (a) Energy landscape of Li/Na atom diffusion along Site 1→Site 2→Site 1 on C_2N-NHG monolayer. The right figures depict the diffusion trajectories of Li/Na from one center of inter-hole to a next center of inter-hole from the top and side views. (b) Energy landscape of Li atom diffusion along Site 4→Site 2 on C_2N-NHG monolayer. The right figures depict the diffusion trajectory of Li from Site 4 to Site 2 from the top and side view. The yellow balls represent Li/Na atoms, and the green balls represent Li atoms.

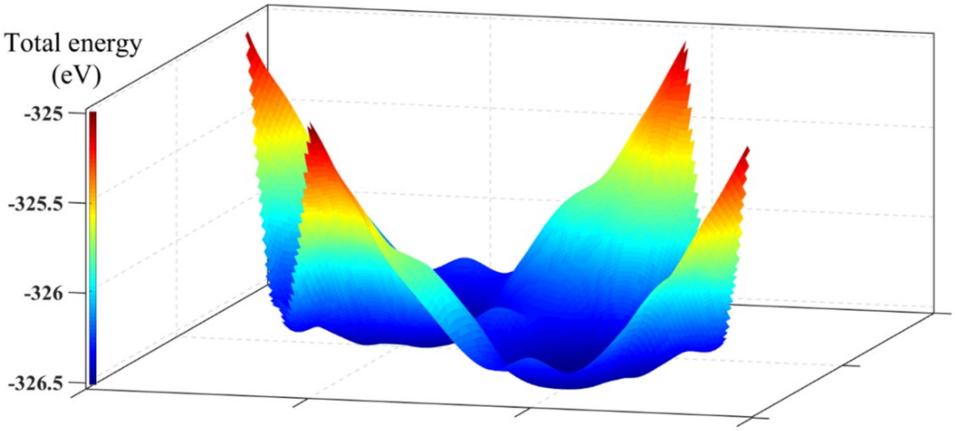

Figure S9. 3D energy profile of double-layered stacking periodic C_2N-NHG unit cell with different layer shifting vectors. The redder color means the higher energy of C_2N-NHG, and the bluer color means the lower energy of C_2N-NHG. The projected plane of the energy landscape is divided by the mesh of 11×11.

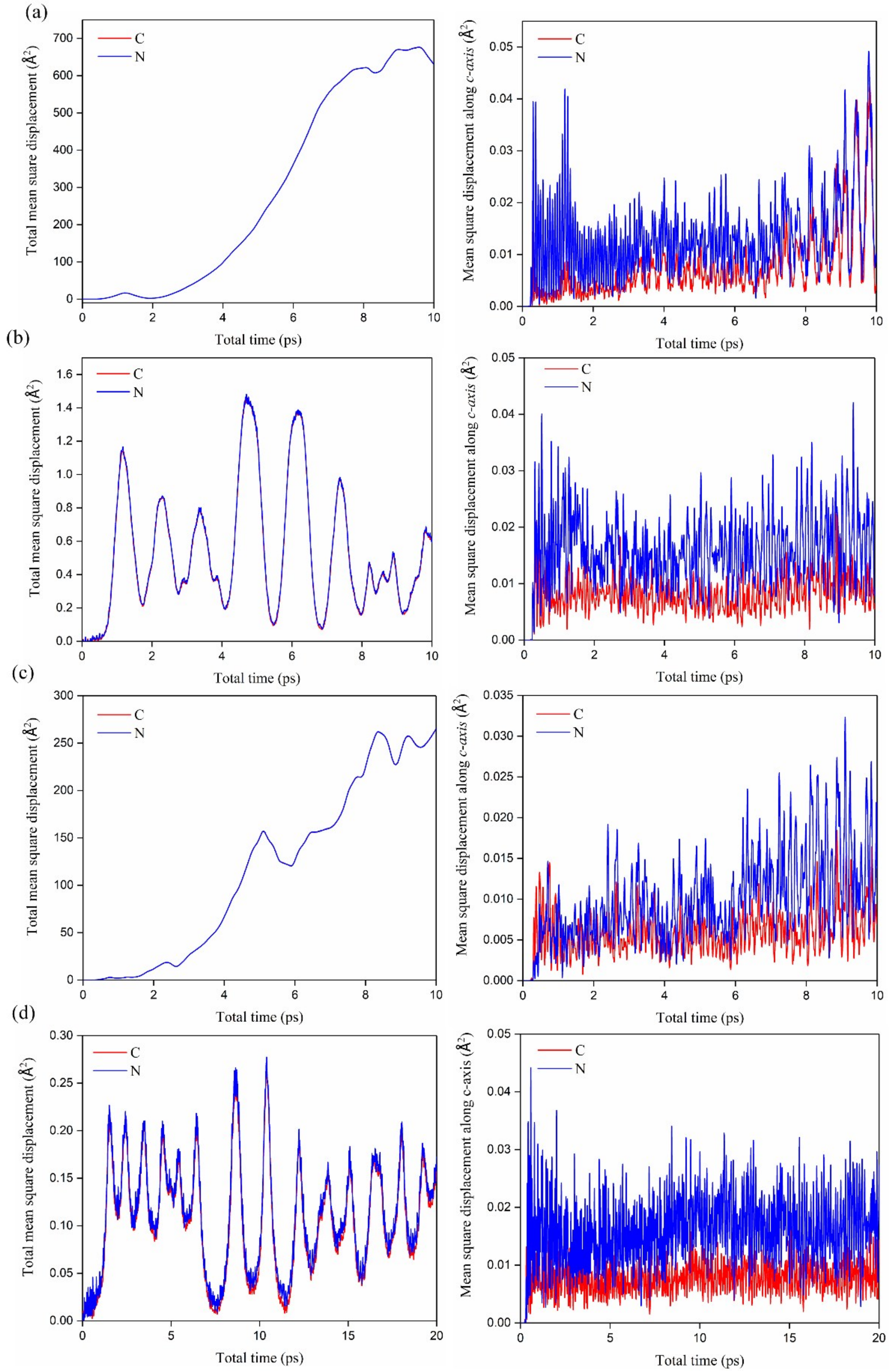

Figure S10. Total mean square displacement and mean square displacement along *c*-axis of all atom species for (a) AA stacking C_2N-NHG, (b) AB stacking C_2N-NHG, (c) AC stacking C_2N-NHG and (d) AD stacking C_2N-NHG.

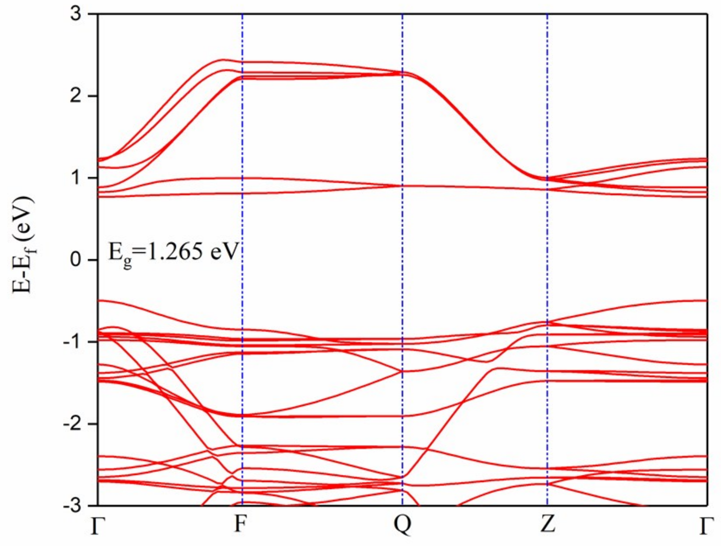

Figure S11. Electronic band structure of AD stacking C_2N-NHG shows a direct band gap of 1.27 eV at the Γ point.

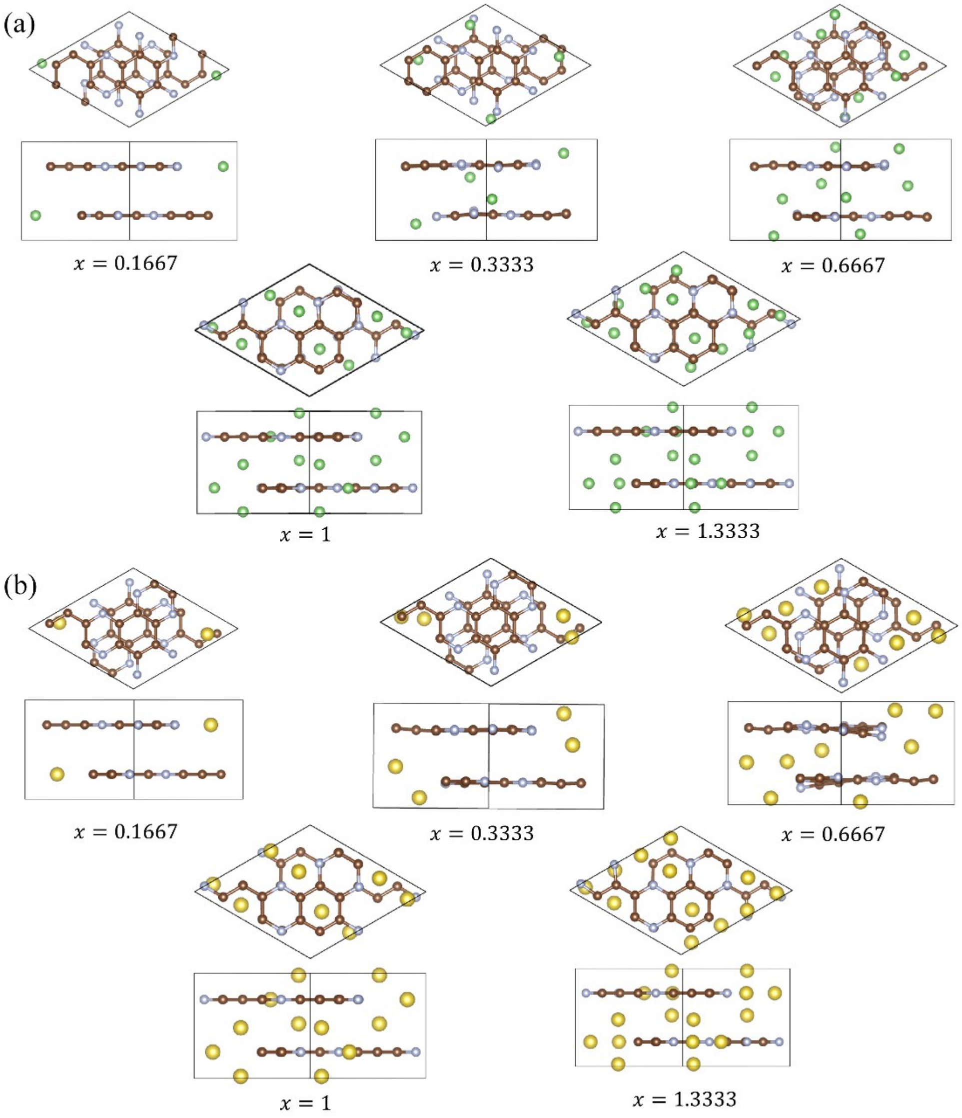

(a) $x = 0.1667$ $x = 0.3333$ $x = 0.6667$ $x = 1$ $x = 1.3333$

(b) $x = 0.1667$ $x = 0.3333$ $x = 0.6667$ $x = 1$ $x = 1.3333$

Figure S12. The most stable structure configurations of Li_x/Na_xC_2N bulk with different concentration of (a) Li metal atoms and (b) Na metal atoms insertion.

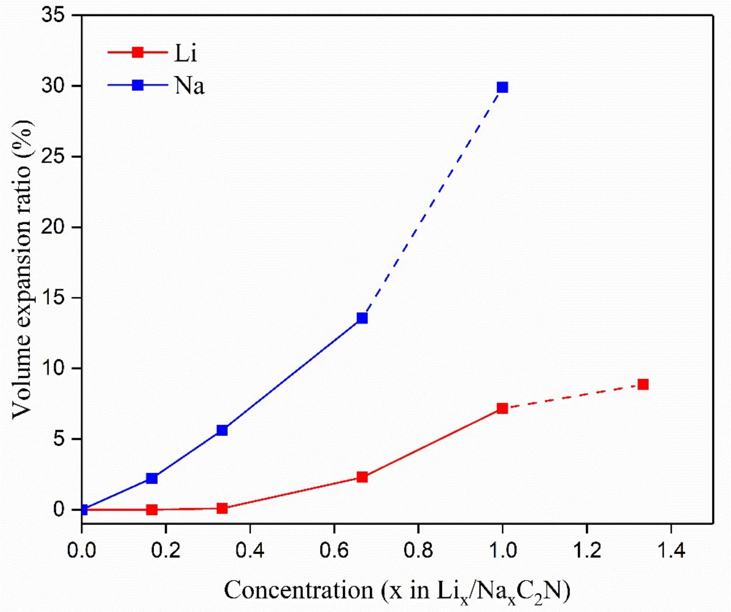

Figure S13. The volume expansion degree of AD stacking C_2N-NHG on different concentration Li and Na atoms insertion.

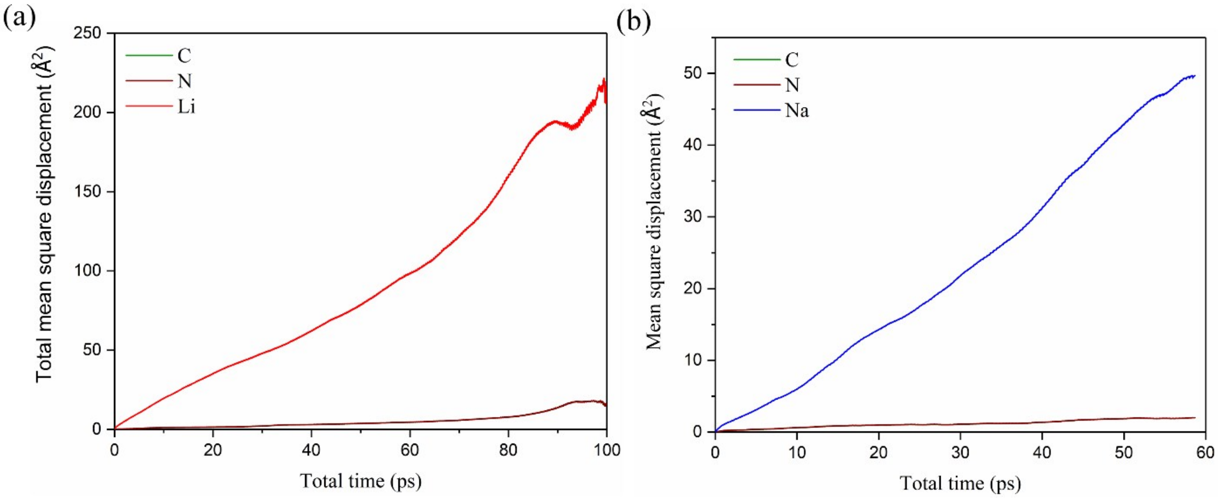

Figure S14. (a) The total mean square displacement of Li, C and N atoms in $Li_{0.67}C_2N$ at 1000K. (b) The total mean square displacement of Na, C and N atoms in $Na_{0.33}C_2N$ at 1000K.

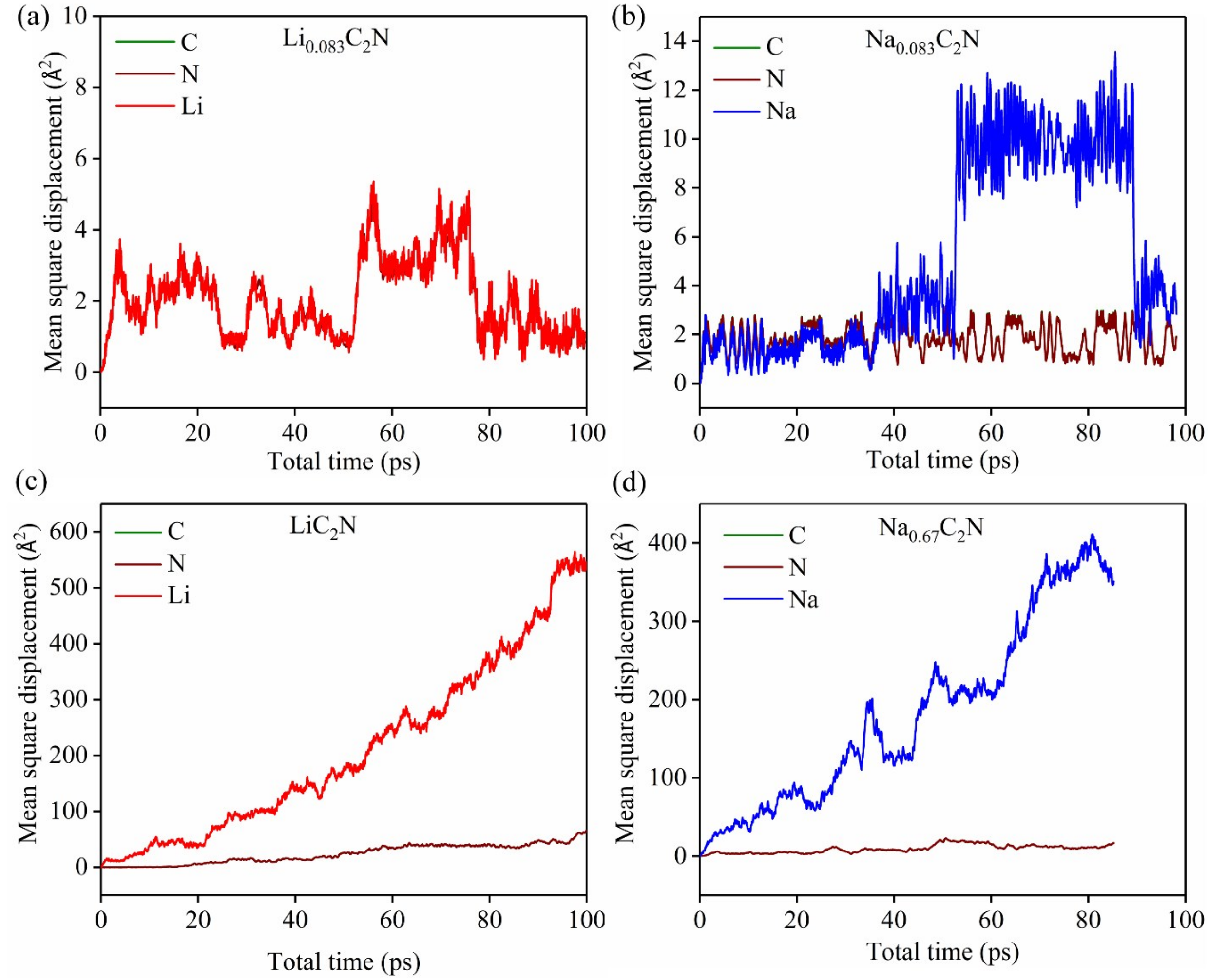

Figure S15. Total mean square displacements of (a) Li, C and N atoms in $Li_{0.083}C_2N$ and (b) Li, C and N atoms in $Na_{0.083}C_2N$ at low state of charge, and (c) Li, C and N atoms in LiC_2N and (b) Li, C and N atoms in $Na_{0.67}C_2N$ at full state of charge. The temperature is set to 1000 K.

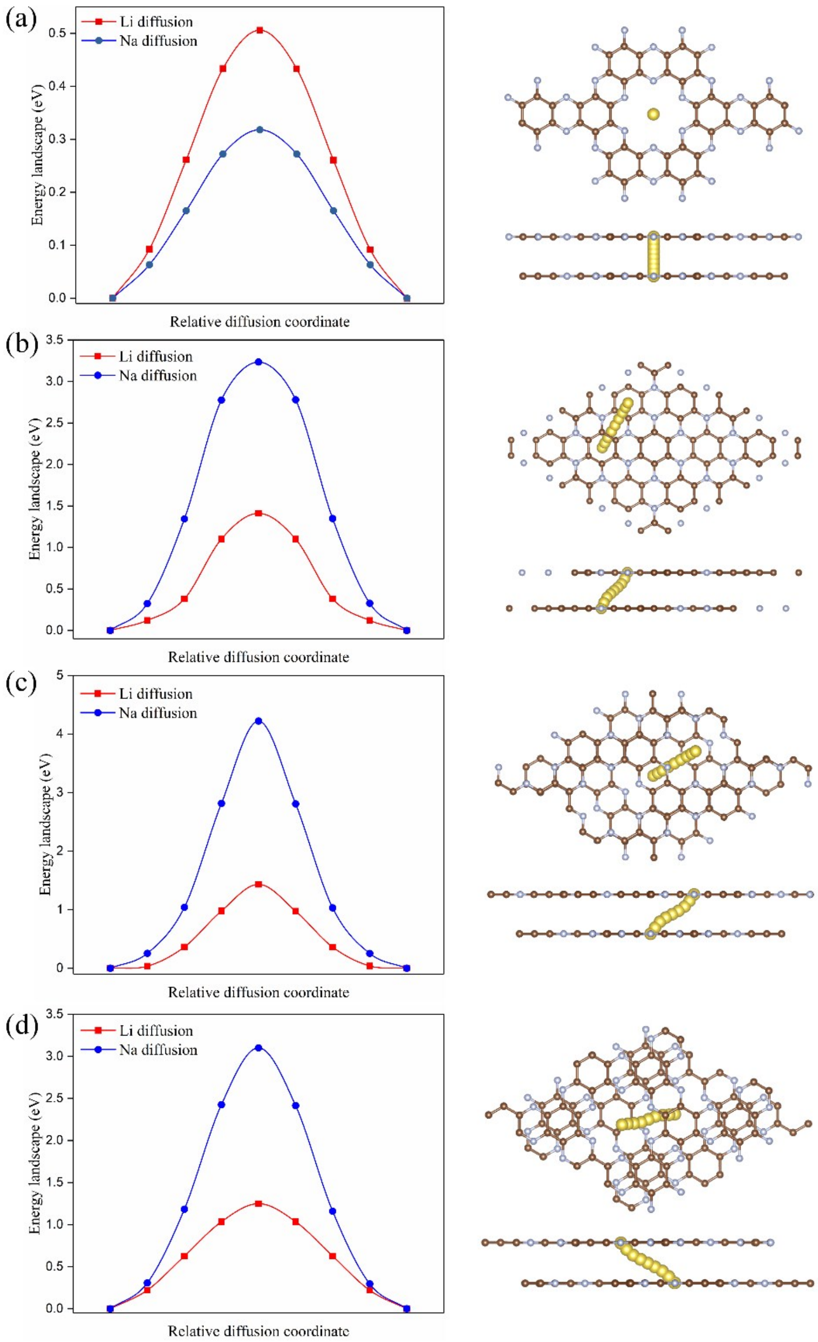

Figure S16. Li and Na single atom migration barriers in AA, AB, AC and AD stacking C_2N-NHG. The brown and silver color balls represent the C and N atoms, respectively, and the yellow color balls represent the transitional Li or Na atoms.

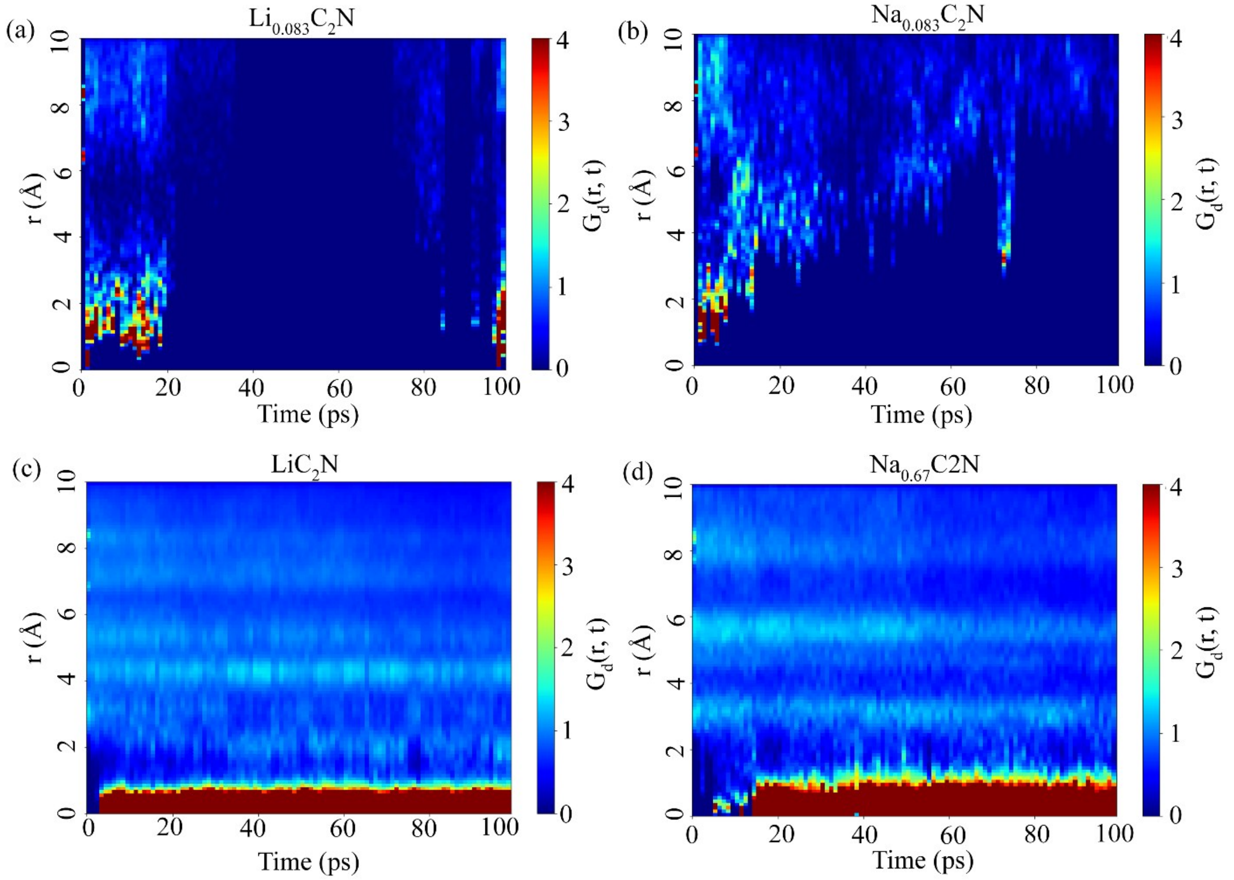

Figure S17. Plots of the distinct-part of the van Hove correlation function (G_d) for (a) $Li_{0.083}C_2N$, (b) $Na_{0.083}C_2N$, (c) LiC_2N and (d) $Na_{0.67}C_2N$ at 1000 K. G_d is a function of the Li-Li or Na-Na pair distance r and time t.

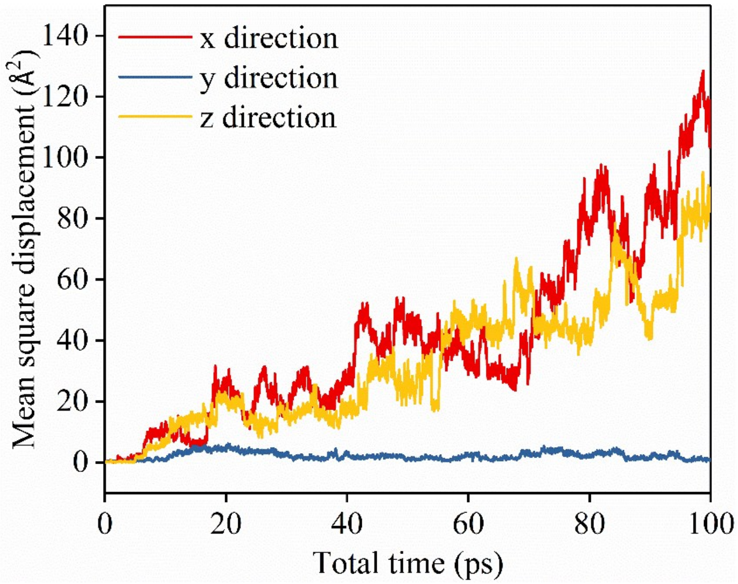

Figure S18. Separated mean square displacement of Li atoms along x direction, y direction and z direction in $Li_{0.67}C_2N$ at 1000 K. The x direction is defined along the *a*-axis, the y direction is perpendicular to the *a*-axis, and the z direction is along the out-of-plane *c*-axis.

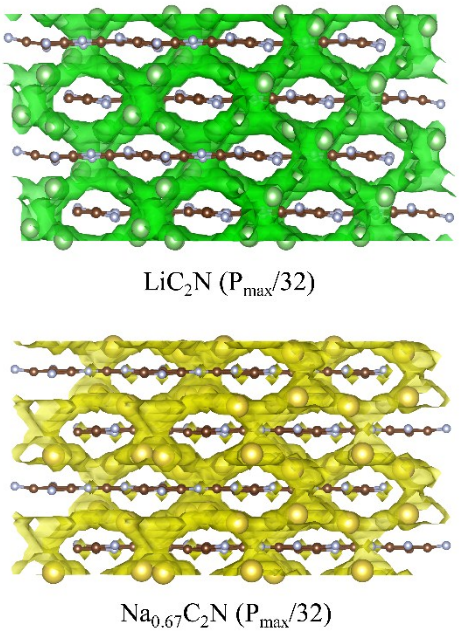

Figure S19. Ionic probability distribution of the Li and Na diffusion networks with an isovalue of $P_{max}/32$ in the fully lithiated LiC_2N and sodiated $Na_{0.67}C_2N$. In the calculations, one Li or Na ion vacancy is introduced, where the C, N, Li, and Na are presented by brown, silver, green, and yellow color balls.

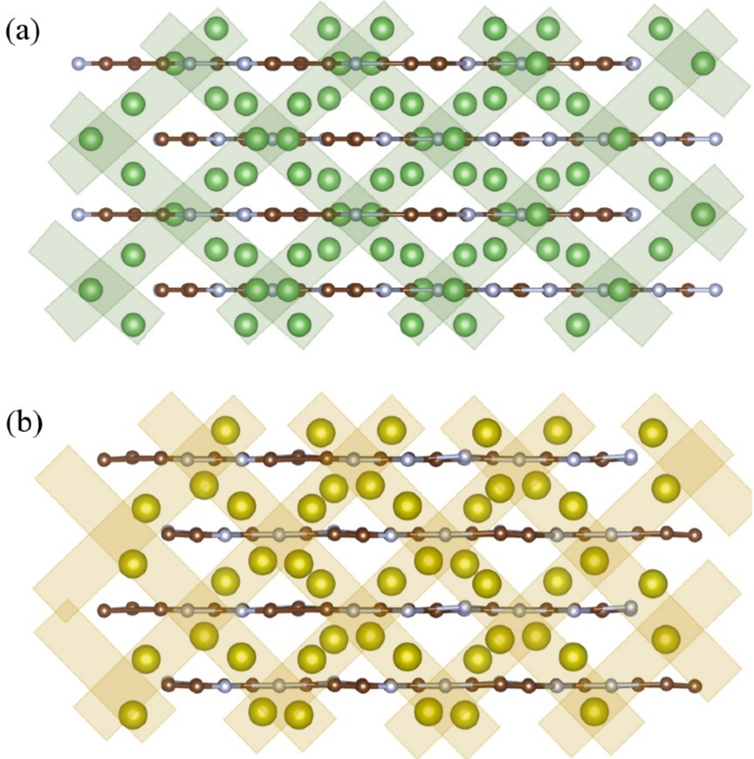

Figure S20. Schematic plot of the potential sites in the AD stacking C_2N-NHG for (a) Li and (b) Na atoms, where small brown and yellow color balls represent C and N atoms, respectively, big green balls in (a) and big yellow balls in (b) are potential Li and Na sites, respectively. The two perpendicular groups of parallel tubes, green in (a) and yellow in (b), represent the zig-zag out-of-plane diffusion channels, which are formed by the inter-holes in the AD stacking C_2N-NHG.

Table S1. Adsorption energies ($E_{ad\text{-}Li}$, $E_{ad\text{-}Na}$) and adsorption distances ($D_{NHG\text{-}Li}$, $D_{NHG\text{-}Na}$) to the C2N-NHG monolayer at four different adsorption sites for Li and Na atoms.

Adsorption site	$E_{ad\text{-}Li}$ (eV)	$D_{NHG\text{-}Li}$ (Å)	$E_{ad\text{-}Na}$ (eV)	$D_{NHG\text{-}Na}$ (Å)
Site 1	-2.690	0	-3.110	0
Site 2	+0.035	1.726	-0.035	2.177

Site 3	+0.259	1.756	+0.104	2.226
Site 4	-2.820	0	-	-

Table S2. The total jumps, collective jumps, tracer diffusivity (D^*) and jump rate diffusivity (D_J) of Li atom and Na atom in $Li_{0.67}C_2N$ and $Na_{0.33}C_2N$ at 800K, 1000K, 1200K and 1400K.

	$Li_{0.67}C_2N$				$Na_{0.33}C_2N$			
	Total jumps (times)	Collective jumps (times)	D^* (m^2/s)	D_J (m^2/s)	Total jumps (times)	Collective jumps (times)	D^* (m^2/s)	D_J (m^2/s)
800 K	93	54	7.76×10^{-10}	4.66×10^{-9}	40	21	5.13×10^{-10}	1.98×10^{-9}
1000 K	158	100	2.24×10^{-9}	7.92×10^{-9}	47	26	1.18×10^{-9}	3.92×10^{-9}
1200 K	210	162	2.32×10^{-9}	1.05×10^{-8}	97	61	1.51×10^{-8}	4.85×10^{-8}
1400 K	268	229	4.70×10^{-9}	1.84×10^{-8}	123	99	2.17×10^{-8}	6.17×10^{-8}

References

1. M. Makaremi, B. Mortazavi and C. V. Singh, *The Journal of Physical Chemistry C*, 2017, **121**, 18575-18583.
2. J. T. Xu, J. Mahmood, Y. H. Dou, S. X. Dou, F. Li, L. M. Dai and J. B. Baek, *Advanced Materials*, 2017, **29**.
3. H. Sahin, *Physical Review B*, 2015, **92**.
4. J. Mahmood, E. K. Lee, M. Jung, D. Shin, I. Y. Jeon, S. M. Jung, H. J. Choi, J. M. Seo, S. Y. Bae, S. D. Sohn, N. Park, J. H. Oh, H. J. Shin and J. B. Baek, *Nature Communications*, 2015, **6**.
5. R. Zhang, B. Li and J. Yang, *Nanoscale,* 2015, **7**, 14062-14070.
6. D. Wu, B. Yang, H. Chen and E. Ruckenstein, *Energy Storage Materials*, 2019, **16**, 574-580.

7. P. Bhauriyal, A. Mahata and B. Pathak, *The Journal of Physical Chemistry C*, 2018, **122**, 2481-2489.
8. J. Zhang, G. Liu, H. Hu, L. Wu, Q. Wang, X. Xin, S. Li and P. Lu, Applied Surface Science 2019, **487**, 1026-1032.
9. Y. G. Zhou and X. T. Zu, *Electrochimica Acta*, 2017, **235**, 167-174.
10. M. Mortazavi, C. Wang, J. K. Deng, V. B. Shenoy and N. V. Medhekar, *Journal of Power Sources*, 2014, **268**, 279-286.